


 Cite this: *RSC Adv.*, 2018, 8, 39371

 Received 2nd September 2018  
Accepted 19th November 2018

DOI: 10.1039/c8ra07326k

rsc.li/rsc-advances

# Enhanced lithium storage performance of V<sub>2</sub>O<sub>5</sub> with oxygen vacancy

 Yinlu Sun,<sup>a</sup> Zhiping Xie<sup>b</sup> and Yanwei Li<sup>id</sup>\*<sup>b</sup>

Orthorhombic phase V<sub>2</sub>O<sub>5</sub> nanosheets with a high V<sup>4+</sup> content (V-V<sub>2</sub>O<sub>5</sub>) have been fabricated *via* a facile sol-gel method and freeze-drying technology followed with a vacuum annealing process. XPS tests demonstrated that the content of V<sup>4+</sup> in the as-prepared V-V<sub>2</sub>O<sub>5</sub> sample was 7.4%, much higher than that (4.7%) in the V<sub>2</sub>O<sub>5</sub> sample annealed in air. Compared with the V<sub>2</sub>O<sub>5</sub> annealed in air, the V-V<sub>2</sub>O<sub>5</sub> sample exhibited better cycling stability, higher lithium storage activity, and smaller electrochemical reaction resistance when evaluated as a cathode active material for lithium ion batteries. For example, the specific capacity of the V-V<sub>2</sub>O<sub>5</sub> and V<sub>2</sub>O<sub>5</sub> electrodes after 100 cycles at 200 mA g<sup>-1</sup> are 224.7 and 199.2 mA h g<sup>-1</sup>, respectively; after 200 cycles at 3 A g<sup>-1</sup> are 150 and 136.7 mA h g<sup>-1</sup>, respectively.

## 1. Introduction

Orthorhombic vanadium pentoxide (V<sub>2</sub>O<sub>5</sub>) has been widely studied in lithium ion battery cathode materials because of its typical lamellar crystal structure.<sup>1</sup> Compared with conventional lithium ion battery cathode materials, V<sub>2</sub>O<sub>5</sub> has much higher theoretical capacity (294 mA h g<sup>-1</sup>, when storing two Li<sup>+</sup>) than other materials. V<sub>2</sub>O<sub>5</sub> also has the advantages of abundant resources, low cost, relatively simple preparation process and good safety.<sup>2-4</sup> However, the drawbacks such as structure instability, low electronic and ionic conductivity and slow electrochemical kinetics drastically reduce its cycling stability and rate capability, which has become the main restrictions to its practical application in the cathode materials of lithium ion batteries.<sup>5,6</sup> To overcome these drawbacks, numerous efforts have been carried out. Some researches mainly concentrate on modifier materials such as various nanostructures V<sub>2</sub>O<sub>5</sub>,<sup>7,8</sup> aliovalent-ion doped V<sub>2</sub>O<sub>5</sub>,<sup>6,9</sup> V<sub>2</sub>O<sub>5</sub> coated with carbon materials or other compounds.<sup>10,11</sup> These modifiers showed enhanced electrochemical kinetics, specific capacity and rate performance than the pristine V<sub>2</sub>O<sub>5</sub> due to their small size and large surface area, which could greatly increase the contact area between actives materials and electrolyte, shorten the diffusion pathways of Li<sup>+</sup>, and relax the mechanical stress associated Li<sup>+</sup> intercalation/deintercalation. However, it should be noted that these modifications are complex, difficult to control and costly.

The heat treatment atmosphere has great influence on the valence state of V element in V<sub>2</sub>O<sub>5</sub>. Generally, when being heat treated in an oxidation atmosphere (such as air and O<sub>2</sub>

atmosphere), the V<sup>4+</sup>/V<sup>5+</sup> ratio and O vacancies in the final V<sub>2</sub>O<sub>5</sub> product are very small; when being heat treated in inert gas (such as Ar atmosphere), and reduction atmospheres (such as H<sub>2</sub> atmosphere), the V<sup>4+</sup>/V<sup>5+</sup> ratio and O vacancies in the final V<sub>2</sub>O<sub>5</sub> product are high, and the V<sub>2</sub>O<sub>5</sub> phase can even transform to VO<sub>2</sub> phase in strong reduction atmosphere. These O vacancies in V<sub>2</sub>O<sub>5</sub> can provide more active sites for the embedding of Li<sup>+</sup>, and increase the specific discharge capacity of the materials. O vacancies can also increase the electronic and ionic conductivity of the materials and promote the lithium storage kinetics.<sup>12-14</sup> However, the preparation process of V<sub>2</sub>O<sub>5</sub> with O vacancy is complex and consumptive, and the electrochemical lithium storage capacity is not satisfactory. It is found that under the condition of oxygen depletion, oxygen can easily escape from the lattice due to the breakage of the V=O bond, resulting in the formation of multiple O vacancies in V<sub>2</sub>O<sub>5</sub> materials.

Herein, we prepared orthorhombic phase V<sub>2</sub>O<sub>5</sub> nanosheets with a high V<sup>4+</sup> content and O vacancies (denoted as V-V<sub>2</sub>O<sub>5</sub>) by a facile sol-gel method combined with freeze drying technique followed with annealing in vacuum. The microstructure of V-V<sub>2</sub>O<sub>5</sub> was analyzed by physical characterizations, and the electrochemical properties of V-V<sub>2</sub>O<sub>5</sub> were evaluated as potential cathode materials for lithium ion batteries (LIBs). The results show that the electrode material has good lithium storage activity, cyclic stability and high current discharge performance.

## 2. Materials and methods

### 2.1 Synthesis of V-V<sub>2</sub>O<sub>5</sub>

All chemical reagents were of analytical purity and used without further purification. The synthesis of V-V<sub>2</sub>O<sub>5</sub> is as following: firstly, commercialized V<sub>2</sub>O<sub>5</sub> powder (C-V<sub>2</sub>O<sub>5</sub>) was added into de-ionized (DI) water and 30 wt% H<sub>2</sub>O<sub>2</sub> to obtain

<sup>a</sup>College of Chemistry, Liaoning University, Shenyang 110036, Liaoning, China

<sup>b</sup>Guangxi Key Laboratory of Electrochemical and Magneto-chemical Functional Materials, College of Chemistry and Bioengineering, Guilin University of Technology, Guilin 541004, Guangxi, China. E-mail: lywhit@126.com


a solution with a  $\text{V}_2\text{O}_5$  concentration of 0.3 M and  $n(\text{H}_2\text{O}_2) : n(\text{V}) = 8 : 1$ . The resulting solution was stirred for 15 min at room temperature. Sonicated for 10 min, the obtained solution was diluted with DI to  $C_V = 0.056$  M. And then the solution was sonicated for about 1 h until it turned into brownish red  $\text{V}_2\text{O}_5$  gel. The gel was stored overnight and diluted with DI water and fully stirred to form a brick-red coloured, transparent sol with  $C_V$  of 0.028 M. Secondly, this solution was pre-frozen in a refrigerator for 1 day and then the solvent (water) in the frozen sample was removed using a freeze dryer (FD-1A-50, Boyikang Corp., Beijing, China) under a vacuum at  $50^\circ\text{C}$  for 2 days to get the  $\text{V}_2\text{O}_5$  precursor. Thirdly, the  $\text{V}_2\text{O}_5$  precursor was annealed in vacuum at  $400^\circ\text{C}$  for 1 h and then annealed at  $400^\circ\text{C}$  in the air for 1 h to form  $\text{V}_2\text{O}_5$  containing O vacancy (denoted as V- $\text{V}_2\text{O}_5$ ). For comparison, the  $\text{V}_2\text{O}_5$  precursor was also annealed in air for 2 h and the final product is denoted as  $\text{V}_2\text{O}_5$ .

## 2.2 Material characterizations

The crystal structure of the prepared samples was determined on X'Pert<sup>3</sup> diffractometer (PANalytical, Netherlands) with a Cu  $K_\alpha$  as radiation source ( $\lambda = 1.54056 \text{ \AA}$ ) in a  $2\theta$  range of  $10\text{--}70^\circ$ . The morphology of the prepared samples was characterized on a field-emission scanning electron microscopy (FE-SEM) (Hitachi, SU-5000) and transmission electron microscope (TEM, JEOL JEM-2100F). The chemical composition and the valence state of V in the prepared samples were analyzed by X-ray photoelectron spectroscopy (XPS) spectrometer (ESCALAB 250Xi) using monochromic Al  $K_\alpha$  excitation.

## 2.3 Electrochemical measurements

The electrochemical performances of the samples were tested using CR 2016 coin-type cell with metallic lithium as the anode and polypropylene (PP) film as the separator. The cathodes were fabricated by mixing V- $\text{V}_2\text{O}_5$ , acetylene black, and poly(vinylidene fluoride) (PVDF) with a weight ratio of 7 : 2 : 1 in *n*-methyl-2-pyrrolidone (NMP) solvent. The resulting slurry was then uniformly spread on an aluminium foil current collector. The cathodes were dried at  $80^\circ\text{C}$  for 12 h in an oven and then punched into small disks with a diameter of 15 mm. The thickness of the electrode was about  $15 \mu\text{m}$  and the mass loading of the active material was about  $1.0 \text{ mg cm}^{-2}$ . The electrolyte was 1 M LiPF<sub>6</sub> in EC/DMC/DEC (1 : 1 : 1 by weight). The cells were galvanostatically charged and discharged between 2.0 and 4.0 V (vs. Li/Li<sup>+</sup>) using LANDCT2001A battery tester at room temperature. Cyclic voltammetry (CV) and electrochemical impedance spectroscopy (EIS) measurements were carried out on an electrochemical workstation (CHI 760). The CV test was performed between 2.0 and 4.0 V at a scan rate of  $0.2 \text{ mV s}^{-1}$ . The EIS was measured was performed in the frequency range from 0.01 Hz to 100 kHz at the open circuit voltage (OCV) after given discharge/charge cycles with 5 mV voltage amplitude.

# 3 Results and discussions

## 3.1 Structure characterization

Fig. 1 presents the XRD patterns of the pure  $\text{V}_2\text{O}_5$  and V- $\text{V}_2\text{O}_5$  samples. Both pure  $\text{V}_2\text{O}_5$  and V- $\text{V}_2\text{O}_5$  samples show a single orthorhombic  $\text{V}_2\text{O}_5$  phase (JCPDS card no. 41-1426) without detectable secondary phase. The peaks around  $2\theta = 15.49^\circ$ ,  $20.35^\circ$ ,  $26.23^\circ$  and  $31.09^\circ$  correspond to (200), (001), (101), (110) diffraction peak of the orthogonal phase  $\text{V}_2\text{O}_5$ . By careful observation, it can be found that there is obvious difference of the relative intensities of (001), (110) and (011) diffraction peaks for the two samples. For V- $\text{V}_2\text{O}_5$ , the intensity ratio between (001) and (110) diffractions and the ratio between (001) and (011) diffractions are 6.2 and 3.3, respectively, which are smaller than those (9.5 and 4.3) of pure  $\text{V}_2\text{O}_5$ . This indicates that the V- $\text{V}_2\text{O}_5$  exposed more facets than the pure  $\text{V}_2\text{O}_5$ . The lattice constants of samples were calculated based on the XRD patterns in Fig. 1 by jade software. For  $\text{V}_2\text{O}_5$ , calculated lattices constants are  $a = 11.484 \text{ \AA}$ ,  $b = 3.556 \text{ \AA}$ ,  $c = 4.357 \text{ \AA}$ ; for V- $\text{V}_2\text{O}_5$ , the calculated lattice constants are  $a = 11.513 \text{ \AA}$ ,  $b = 3.564 \text{ \AA}$ ,  $c = 4.372 \text{ \AA}$ . It can be seen that the V- $\text{V}_2\text{O}_5$  shows slight lattice expansions as compared to that of  $\text{V}_2\text{O}_5$ . It is known that radius of  $\text{V}^{4+}$  is larger than that of  $\text{V}^{5+}$ . Therefore, the lattice expansion can be attributed to the increased  $\text{V}^{4+}$  content in V- $\text{V}_2\text{O}_5$  sample (Fig. 3).

Fig. 2 gives the SEM and TEM images of the pure  $\text{V}_2\text{O}_5$  and V- $\text{V}_2\text{O}_5$  samples. It can be seen that both V- $\text{V}_2\text{O}_5$  and  $\text{V}_2\text{O}_5$  are 2D sheet-like morphologies. By observing the high magnification SEM and TEM images, the surface of the V- $\text{V}_2\text{O}_5$  has a lot of deeper ravines and the surface fluctuates greatly (Fig. 2c, g and h), while  $\text{V}_2\text{O}_5$  is a flat sheet with cracks attributed to the mechanical force in the sample preparation process (Fig. 2f, j and k). Compared with pure  $\text{V}_2\text{O}_5$ , the coarse surface of V- $\text{V}_2\text{O}_5$  is more effective to inhibit the stacking of sheets, store more electrolyte, offer larger material-electrolyte contact area, and relax the mechanical strain generated upon the lithium ion intercalation/deintercalation cycles. The lattice fringe (inset of Fig. 2i and l) of about  $4.36 \text{ \AA}$  can be assigned to the (001) plane of orthorhombic  $\text{V}_2\text{O}_5$ , consistent with the XRD patterns shown in Fig. 1.

XPS was carried out to investigate the oxidation state of vanadium and O vacancies in V- $\text{V}_2\text{O}_5$  and  $\text{V}_2\text{O}_5$  samples. The

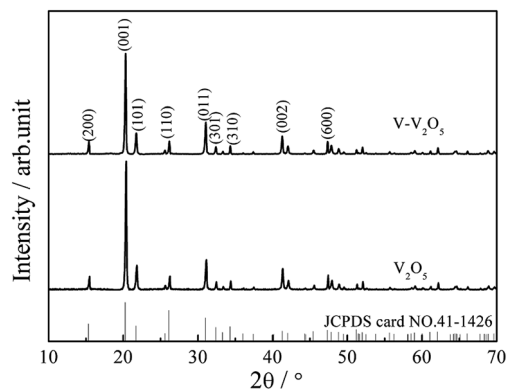


Fig. 1 XRD patterns of the V- $\text{V}_2\text{O}_5$  and  $\text{V}_2\text{O}_5$  samples.



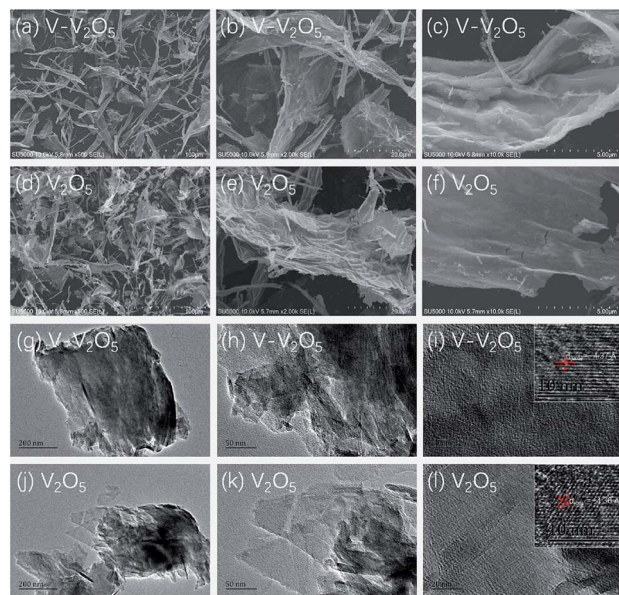


Fig. 2 FESEM images of the V-V<sub>2</sub>O<sub>5</sub> (a–c) and V<sub>2</sub>O<sub>5</sub> (d–f) samples; TEM images of the V-V<sub>2</sub>O<sub>5</sub> (g–i) and V<sub>2</sub>O<sub>5</sub> (j–l) samples.

V2p<sub>3/2</sub> spectra shown in Fig. 3 compose of two components locating at the binding energy values of 517.6 and 516.3 eV, which are associated with two formal oxidation degrees, V<sup>5+</sup> and V<sup>4+</sup>.<sup>15,16</sup> From the area ratio of the fitted spectrum of V<sup>5+</sup> and V<sup>4+</sup>, the molar ratios of V<sup>4+</sup>/(V<sup>4+</sup> + V<sup>5+</sup>) in V-V<sub>2</sub>O<sub>5</sub> and V<sub>2</sub>O<sub>5</sub> are 7.4% and 4.7%, respectively. According to charge neutrality of system, the formation of one O vacancy should corresponds the generation of two V<sup>4+</sup>. Thus, the O vacancies concentrations in V-V<sub>2</sub>O<sub>5</sub>

and V<sub>2</sub>O<sub>5</sub> are calculated to be 3.7% and 2.35%, respectively. The increased of V<sup>4+</sup> content in V-V<sub>2</sub>O<sub>5</sub> can be attribute to the loss of lattice O in V<sub>2</sub>O<sub>5</sub> during the annealing process in oxygen depletion condition (vacuum). The present of oxygen vacancies could leave more open voids, which will provide more migration paths for the fast Li<sup>+</sup> diffusion and facilitate the reversible phase transitions of V<sub>2</sub>O<sub>5</sub> during the Li<sup>+</sup> insertion/extraction process.<sup>12,17</sup> Furthermore, it has been suggested that the mixed valence V<sup>4+</sup>/V<sup>5+</sup> could improve the electrical conductivity of the material due to the synergic activity in V<sub>2</sub>O<sub>5</sub> materials.

### 3.2 Electrochemical performances

Fig. 4 show the CV profiles of the first and the fifth cycles at a scan rate of 0.2 mV s<sup>-1</sup> for the pure V<sub>2</sub>O<sub>5</sub> and V-V<sub>2</sub>O<sub>5</sub> electrodes, respectively. As seen from Fig. 4a, for pure V<sub>2</sub>O<sub>5</sub> and V-V<sub>2</sub>O<sub>5</sub> in the first cycle, three reduction peaks at 3.35, 3.10 and 2.20 V are observed, which correspond to the α/ε, ε/δ and δ/γ phase transitions, respectively. During the Li<sup>+</sup> deintercalation process, four oxidation peaks are observed for two samples. The peak at 2.51 V corresponds to the γ/δ phase transition, the peak at 3.24 and 3.35 V correspond to the δ/ε phase transition, and the peak at 3.47 V corresponds to the ε/α phase transition.<sup>18–20</sup> However, after the first intercalation process, the irreversible γ' phase of V<sub>2</sub>O<sub>5</sub> is indicated by the emergence of oxidation peak at 3.65 V and reduction peaks broadening at 2.22 V.<sup>19,21</sup> After 50 cycles in Fig. 4b, the reduction peak currents of the V-V<sub>2</sub>O<sub>5</sub> and V<sub>2</sub>O<sub>5</sub> decrease at 3.16 V while increase at 3.54 V in the γ' intercalation process; simultaneously, the two oxidation peaks corresponding to δ/ε phase transition decrease at 3.24 and

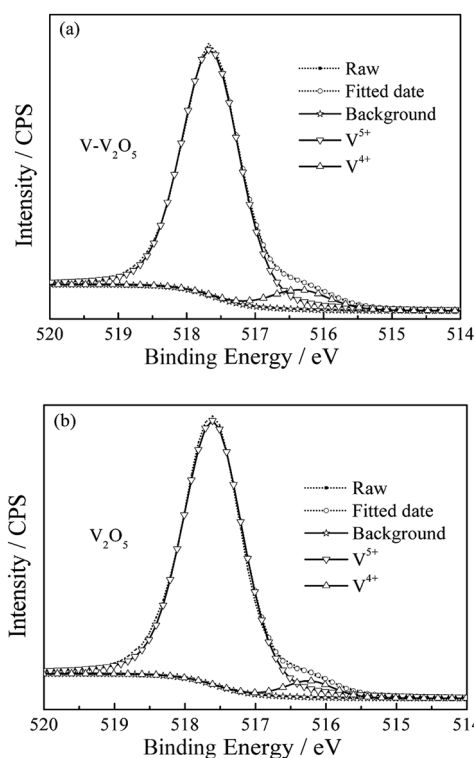


Fig. 3 XPS spectra on V2p<sub>3/2</sub> of (a) V-V<sub>2</sub>O<sub>5</sub> and (b) V<sub>2</sub>O<sub>5</sub> samples.

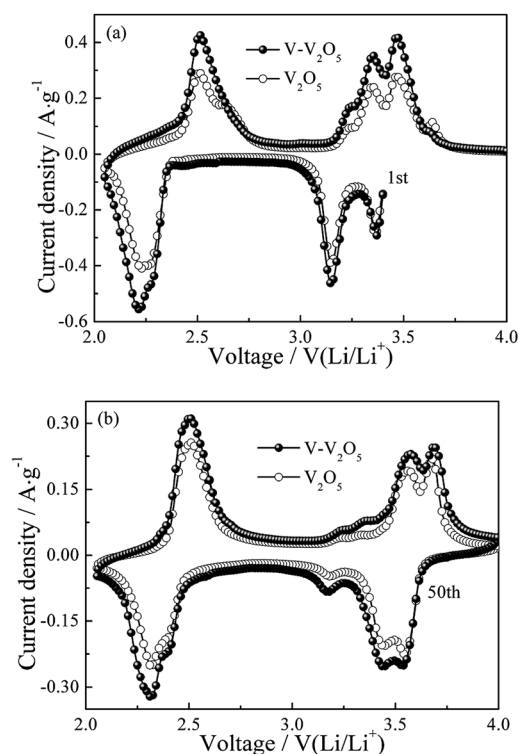


Fig. 4 The (a) first and (b) fifth cycles of CV curves of V-V<sub>2</sub>O<sub>5</sub> and V<sub>2</sub>O<sub>5</sub> electrodes at a scan rate of 0.2 mV s<sup>-1</sup>.



3.35 V while increase at 3.65 V. Additionally, the peak area of V-V<sub>2</sub>O<sub>5</sub> is always greater than that of pure V<sub>2</sub>O<sub>5</sub>, which indicates that the V-V<sub>2</sub>O<sub>5</sub> sample obtained by vacuum annealing has a higher lithium storage activity.

Fig. 5a gives the cycling response of the V-V<sub>2</sub>O<sub>5</sub> and pure V<sub>2</sub>O<sub>5</sub> electrodes at a current density of 200 mA g<sup>-1</sup>. Obviously, V-V<sub>2</sub>O<sub>5</sub> electrode exhibits higher discharge capacity than the pure V<sub>2</sub>O<sub>5</sub> electrode. The maximum discharge specific capacities of V-V<sub>2</sub>O<sub>5</sub> and V<sub>2</sub>O<sub>5</sub> samples are 230.2 and 256.6 mA h g<sup>-1</sup>, respectively. The discharge specific capacities after 50 cycles are 213.1 and 237.9 mA h g<sup>-1</sup>, and after 100 cycles are 199.2 and 224.7 mA h g<sup>-1</sup>, respectively. The intercalation/deintercalation lithium capacity of V-V<sub>2</sub>O<sub>5</sub> is always higher than that of V<sub>2</sub>O<sub>5</sub>. This change of discharge capacity is in accordance with the CV results (Fig. 4). The capacity retention of V-V<sub>2</sub>O<sub>5</sub> electrode at 100<sup>th</sup> cycle is 87.6%, superior to that reported in the literatures on the hydrogenated V<sub>2</sub>O<sub>5</sub> prepared by the H<sub>2</sub> reduction (84% at 100 mA g<sup>-1</sup> and 100<sup>th</sup> cycle),<sup>13</sup> on the V<sub>2</sub>O<sub>5</sub> nanorods prepared by the electrostatic spinning method (43% at 50 mA g<sup>-1</sup> and 50<sup>th</sup> cycle)<sup>22</sup> and on the carbon coated V<sub>2</sub>O<sub>5</sub> nanoparticles (82% at 29.4 mA g<sup>-1</sup> and 30<sup>th</sup> cycle),<sup>10</sup> indicating an excellent capacity retention capability.

Fig. 5b presents the differential capacity corresponding to the cyclic performance of V-V<sub>2</sub>O<sub>5</sub> in Fig. 5a. During the first discharge, the three peaks at 3.37, 3.2 and 2.32 V correspond to the  $\alpha/\epsilon$ ,  $\epsilon/\delta$  and  $\delta/\gamma$  phase transitions, respectively, in accordance with the reduction peaks in CV curve (Fig. 4a); during the charging process, the peak at 2.45 V corresponds to the  $\gamma/\delta$  phase transition, the peak at 3.23 and 3.30 V correspond to the  $\delta/\epsilon$  phase transition, and the peak at 3.43 V corresponds to the  $\epsilon/\alpha$  phase transition, in accordance with the oxidation peaks in CV curve (Fig. 4a). With the increase of charge/discharge the phase transition between  $\epsilon$  phase and  $\delta$  phase decreases gradually, while the intensities of peaks at 3.57 V upon the lithium ion intercalation cycle and at 3.65 V upon the lithium ion deintercalation cycle are gradually

increased. This observation is in good agreement with the CV results.

In order to further study the cyclic stability of V-V<sub>2</sub>O<sub>5</sub> under high current, the cyclic properties of V-V<sub>2</sub>O<sub>5</sub> and V<sub>2</sub>O<sub>5</sub> samples were compared at 1 and 3 A g<sup>-1</sup> current densities, respectively (Fig. 5c and d). At 1 A g<sup>-1</sup>, the discharge specific capacity of V-V<sub>2</sub>O<sub>5</sub> and V<sub>2</sub>O<sub>5</sub> rises first and then decreases, and the maximum capacities are 218.4 and 200.6 mA h g<sup>-1</sup>, respectively. The significantly improved capacity in the first few cycles during cycling measurement can be attributed the activation of electrode (the penetration of electrolyte and/or increase of active surface). The discharge specific capacities of V-V<sub>2</sub>O<sub>5</sub> and V<sub>2</sub>O<sub>5</sub> after 200 cycles are 189.3 and 172.4 mA h g<sup>-1</sup>, respectively. When the current density increases to 3 A g<sup>-1</sup>, the capacity of two electrodes increase gradually and remain stable. The maximum discharge specific capacities of V-V<sub>2</sub>O<sub>5</sub> and V<sub>2</sub>O<sub>5</sub> are 150 and 141.7 mA h g<sup>-1</sup>, respectively. The excellent lithium storage performance of V-V<sub>2</sub>O<sub>5</sub> could be ascribed to the vacuum annealing process. Under the condition of oxygen poor, V<sub>2</sub>O<sub>5</sub> easily loses the O in the crystal structure and forms the O vacancies. The O vacancies can help reduce V<sup>5+</sup> to V<sup>4+</sup>, which increases the electronic and ionic conductivity of the material and also provide additional embedding position for the lithium ion.

The Nyquist impedance spectra of V-V<sub>2</sub>O<sub>5</sub> and V<sub>2</sub>O<sub>5</sub> are shown in Fig. 6, measured at fully discharged state under 200 mA g<sup>-1</sup> in 100th cycles. The Nyquist plots were fitted using an analogical equivalent circuit. In this equivalent circuit,  $R_s$  corresponds to the equivalent series resistance (ESR) which contains all ohmic resistance due to the electrolyte and other parts of the system. Charge transfer resistance ( $R_{ct}$ ) represents the charge-transfer impedance at the electrode/electrolyte interface, corresponding to the semicircles in high-medium frequency scope.  $W$  refers to the Warburg impedance, corresponding to the inclined line in the low-frequency scope. A constant phase element (CPE) is used in the equivalent circuit instead of a pure capacitance due to the inhomogeneous surface of the working electrode. The solid line represents the impedance calculated using the equivalent circuit and the error between the experimental and fitting data was less than 1%. Note that the depressed semicircles related to the charge transfer in the high-medium frequency region and the angled

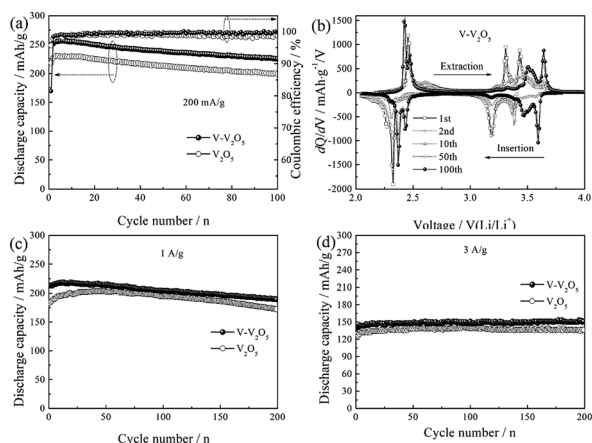


Fig. 5 (a) Cycling performance and coulombic efficiencies of the V-V<sub>2</sub>O<sub>5</sub> and V<sub>2</sub>O<sub>5</sub> electrodes at a current density of 200 mA g<sup>-1</sup>; (b) differential specific capacity plots of the V-V<sub>2</sub>O<sub>5</sub> at different cycle number at a current density of 200 mA g<sup>-1</sup>; cycling performance of V-V<sub>2</sub>O<sub>5</sub> and V<sub>2</sub>O<sub>5</sub> at a current density of (c) 1 A g<sup>-1</sup> and (d) 3 A g<sup>-1</sup>, respectively.

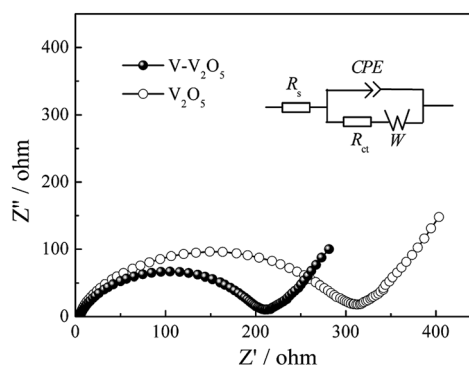


Fig. 6 Nyquist plots of V-V<sub>2</sub>O<sub>5</sub> and V<sub>2</sub>O<sub>5</sub> electrodes.



straight line corresponding to the low frequency range can be effectively simulated. The fitting parameters of the semicircle can be calculated from the corresponding equivalent circuit. The  $R_{ct}$  values of  $V-V_2O_5$  and  $V_2O_5$  are 213.1 and 320.6  $\Omega$ , respectively. It evidently implies that  $V-V_2O_5$  possesses higher electrochemical reaction kinetics, which is ascribed to its O vacancies facilitating lithium insertion/extraction.

## 4 Conclusions

The orthorhombic phase  $V_2O_5$  ( $V-V_2O_5$ ) nanosheet with O vacancies was prepared by a facile sol-gel method combined with freeze drying technique followed with annealing in vacuum. XRD analysis revealed that the relative intensities of (110) and (011) diffraction peaks for  $V-V_2O_5$  were enhanced, and  $V-V_2O_5$  showed slight lattice expansions due to O vacancies. FESEM demonstrated that  $V-V_2O_5$  was 2D sheet-like morphology with coarse surface. XPS tests indicated that O vacancies induced more  $V^{4+}$  in  $V_2O_5$ . When used as cathode material for Li-ion batteries, the  $V-V_2O_5$  exhibited much enhanced rate capability and cycling stability as compared to the pure  $V_2O_5$  counterpart. The superior lithium storage performance of the  $V-V_2O_5$  could be ascribed to the following reasons: coarse surface improves the specific surface area of the nanosheet, and increases the effective contact area between electrode and electrolyte; the predominantly exposed (110) and (011) crystal planes of  $V-V_2O_5$  provide channels for facile  $Li^+$  intercalation and deintercalation, which contributes to the enhanced rate capability; the increased low valence state  $V^{4+}$  may improve the conductivity of  $V-V_2O_5$  and decrease electrochemical reaction resistance. Furthermore, the results indicated that the synergistic effect of  $V^{4+}$  and oxygen vacancy will improve the structure integrity and enhance the diffusion of Li ion. It enlightens us that adjusting the proportion of different valance state of metal elements in metallic oxides is a promising approach for improving their lithium storage for LIBs.

## Conflicts of interest

There are no conflicts to declare.

## Acknowledgements

This work was supported by the financial supports from the National Natural Science Foundation of China (No. 51664012, 51464009 and 51562006), Guangxi Natural Science Foundation of China (2017GXNSFAA198117 and 2015GXNSFGA139006) and Guangxi Key Laboratory of Electrochemical and Magnetochemical Functional Materials (EMFM20181117).

## References

- 1 T. Kim, J. Shin, T. S. You, H. Lee and J. Kim, Thermally controlled  $V_2O_5$  nanoparticles as cathode materials for lithium-ion batteries with enhanced rate capability, *Electrochim. Acta*, 2015, **164**, 227–234.
- 2 D. McNulty, D. N. Buckley and C. O'dwyer, Synthesis and electrochemical properties of vanadium oxide materials and structures as Li-ion battery positive electrodes, *J. Power Sources*, 2014, **267**(4), 831–873.
- 3 Y. Wang and G. Z. Cao, Synthesis and enhanced intercalation properties of nanostructured vanadium oxides, *Chem. Mater.*, 2006, **18**(12), 2787–2804.
- 4 X. Huang, X. H. Rui, H. H. Hng and Q. Y. Yan, Vanadium pentoxide-based cathode materials for lithium-ion batteries: Morphology control, carbon hybridization, and cation doping, *Part. Part. Syst. Charact.*, 2015, **32**(3), 276–294.
- 5 A. Q. Pan, H. B. Wu, L. Zhang and X. W. Lou, Uniform  $V_2O_5$  nanosheet-assembled hollow microflowers with excellent lithium storage properties, *Energy Environ. Sci.*, 2013, **6**(5), 1476–1479.
- 6 Y. W. Li, J. H. Yao, E. Uchaker, M. Zhang, J. J. Tian, X. Y. Liu and G. Z. Cao, Sn-doped  $V_2O_5$  film with enhanced lithium-ion storage performance, *J. Phys. Chem. C*, 2013, **117**(45), 23507–23514.
- 7 J. F. Huang, X. N. Qiao, Z. W. Xu, H. B. Ouyang and J. Y. Li,  $V_2O_5$  nanoflowers assembled by nanorods as cathode material for lithium-ion batteries, *Micro Nano Lett.*, 2015, **10**(12), 686–688.
- 8 H. Y. Wu, M. L. Qin, X. L. Li, Z. Q. Cao, B. R. Jia, Z. L. Zhang, D. Y. Zhang, X. H. Qu and A. A. Volinsky, One step synthesis of vanadium pentoxide sheets as cathodes for lithium ion batteries, *Electrochim. Acta*, 2016, **206**, 301–306.
- 9 H. Yu, X. Rui, H. Tan, J. Chen, X. Huang, C. Xu, W. Liu, D. Y. Yu, H. H. Hng and H. E. Hoster, Cu doped  $V_2O_5$  flowers as cathode material for high-performance lithium ion batteries, *Nanoscale*, 2013, **5**(11), 4937–4943.
- 10 J. Shin, H. Jung, Y. Kim and J. Kim, Carbon-coated  $V_2O_5$  nanoparticles with enhanced electrochemical performance as a cathode material for lithium ion batteries, *J. Alloys Compd.*, 2014, **589**(4), 322–329.
- 11 S. Tian, A. Xing, H. Tang, Z. H. Bao and G. M. Wu, Enhanced cycling stability of TiO-coated V O nanorods through a surface sol-gel process for lithium ion battery applications, *J. Mater. Chem. A*, 2014, **2**(9), 2896–2900.
- 12 H. Q. Song, C. F. Liu, C. K. Zhang and G. Z. Cao, Self-doped  $V^{4+}$ - $V_2O_5$  nanoflake for 2 Li-ion intercalation with enhanced rate and cycling performance, *Nano Energy*, 2016, **22**, 1–10.
- 13 X. Peng, X. M. Zhang, L. Wang, L. S. Hu, S. H. S. Cheng, C. Huang, B. Gao, F. Ma, K. F. Huo and P. K. Chu, Hydrogenated  $V_2O_5$  nanosheets for superior lithium storage properties, *Adv. Funct. Mater.*, 2016, **26**(5), 784–791.
- 14 D. W. Liu, Y. Y. Liu, A. Q. Pan, K. P. Nagle, G. T. Seidler, Y. H. Jeong and G. Z. Cao, Enhanced Lithium-Ion Intercalation Properties of  $V_2O_5$  Xerogel Electrodes with Surface Defects, *J. Phys. Chem. C*, 2011, **115**(11), 4959–4965.
- 15 M. Demeter, M. Neumann and W. Reichelt, Mixed-valence vanadium oxides studied by XPS, *Surf. Sci.*, 2000, **454**(12), 41–44.
- 16 A. Benayad, H. Martinez and A. Gies, XPS investigations achieved on the first cycle of  $V_2O_5$  thin films used in lithium microbatteries, *J. Electron Spectrosc. Relat. Phenom.*, 2006, **150**(1), 1–10.



- 17 D. W. Liu, Y. Y. Liu, B. B. Garcia, Q. F. Zhang, A. Q. Pan, Y. H. Jeong and G. Z. Cao,  $V_2O_5$  xerogel electrodes with much enhanced lithium-ion intercalation properties with  $N_2$  annealing, *J. Mater. Chem.*, 2009, **19**(46), 8789–8795.
- 18 X. T. Gao, X. D. Zhu, S. R. Le, D. J. Yan, C. Y. Qu, Y. J. Feng, K. N. Sun and Y. T. Liu, Boosting High-Rate Lithium Storage of  $V_2O_5$  Nanowires by Self-Assembly on N-Doped Graphene Nanosheets, *ChemElectroChem*, 2016, **3**(11), 1730–1736.
- 19 G. Q. Jia, Z. N. Deng, X. Liu, H. Jiang and C. Z. Li, Building radially oriented architecture by tailorable  $V_2O_5$  nanoribbons toward enhanced lithium storage, *Chem. Eng. J.*, 2016, **304**, 194–200.
- 20 M. Przeźniak-Welenc, J. Karczewski, J. Smalc-Koziorowska, M. Łapiński, W. Sadowski and B. Kościelska, The influence of nanostructure size on  $V_2O_5$  electrochemical properties as cathode materials for lithium ion batteries, *RSC Adv.*, 2016, **6**(61), 55689–55697.
- 21 Y. W. Li, J. H. Yao, E. Uchaker, J. W. Yang, Y. X. Huang, M. Zhang and G. Z. Cao, Leaf-like  $V_2O_5$  nanosheets fabricated by a facile green approach as high energy cathode material for lithium-ion batteries, *Adv. Energy Mater.*, 2013, **3**(9), 1171–1175.
- 22 C. C. Zhu, J. Shu, X. Z. Wu, P. Li and X. Li, Electrospun  $V_2O_5$  micro/nanorods as cathode materials for lithium ion battery, *J. Electroanal. Chem.*, 2015, **759**, 184–189.

